BHR Group
EXPERTS IN FLUID ENGINEERING

Machinability of Randomly Chopped Discontinuous Fiber Composites: A Comparative Assessment of Conventional and Abrasive Waterjet

Rishi Pahuja[1] and M. Ramulu[1]
[1]Department of Mechanical Engineering, University of Washington Box 352600 Seattle, WA 98195, U.S.A.

Keywords: AWJ, Discontinuous fiber composites, surface roughness, HexMC

Abstract

This study evaluates the machinability of HexMC® composite consisting of chopped and randomly distributed graphite-epoxy unidirectional prepeg tapes. Abrasive waterjet was employed with varied pressure, traverse feed and abrasive flow rate to study the parametric effects on the kerf characteristics – surface roughness and kerf width, and material removal rate as a function of jet penetration depth. Predictive empirical models were developed along-with the sensitivity analysis, identifying the major contributing parameter(s). To identify the differences in surface generated through AWJ and conventional machining, the workpiece was conventionally trimmed with same traverse feed levels. A comparative evaluation of the surface quality was made through surface profilometry and microscopic inspection. The study specifically focused on microscopic inspection and characterization of machining induced damages and defects in HexMC composite material.

Notation

P	Water pressure	R	Load ratio
u	Traverse speed	C_d	Coefficient of drag
AFR ($\dot{m}_a$)	Abrasive flow rate	d_0	Orifice diameter
MRR	Material removal rate	A_0	Orifice cross-sectional area
P_{awj}	Abrasive waterjet power	ρ_w	Water density
P_{wj}	Waterjet power	d_n/ d_m	Nozzle diameter
v_w	Water velocity	η	Power efficacy
W	Kerf width	E_{sp}	Specific jet energy

1. INTRODUCTION

HexMC is composed of slit prepreg tapes, chopped, randomly distributed and compression molded in thermoset epoxy resin. The high strength and specific modulus, ease of formability, low production cost qualify HexMC as a primary candidate for geometrically complex, secondary structural elements such as aircraft window frames of Boeing 787 Dreamliner [1] . HexMC is an ideal replacement for weight saving alloys: Titanium, Magnesium and Aluminum. Although HexMC is molded to a near net shape, often times secondary machining such as drilling, reaming and trimming is unavoidable. Over time, several researches have reported challenges in conventional machining or finishing of polymer matrix composites such as CFRP (Carbon Fiber Reinforced Composites) and GFRP (Glass Fiber Reinforced Composites) due to high tool wear, delamination and damages, fraying and environmentally malign dust creation. All these issues have led to the adoption of non-traditional machining practices such as waterjet, ultrasonic, electrical discharge and laser machining. Among all, Abrasive Waterjet (AWJ) is one of the most feasible alternatives for machining composites primarily due to the absence of thermal damage and tool wear.

Several studies have been reported in the area of pure and abrasive waterjet machining of thermoplastic polymer matrix composites infiltrated with continuous fibers. Arola et al. [2] investigated the material removal mechanism in AWJ machining of unidirectional graphite/epoxy composite and observed the abrasive wear tracks near top kerf and high delamination at jet exit side along with extensive fiber pull-out. Top kerf width was found greater than pure waterjet. Fibers were machined by non-repeated fractures by shearing and micro-machining action of abrasives. Microbending delamination of matrix material was observed at the jet exit side. The study suggested better performance of Abrasive waterjet cutting over pure waterjet due to high degree of damage such as hydrowedging, delamination and high surface roughness involved with pure waterjet. Hashish [3] studied the machining of a wide range of advanced composites and concluded the inability of pure waterjet in machining thick composites, and reported higher delamination at low pressure and high traverse rates. Wang [4] studied the machinability of 3 mm thick polymer matrix composites in terms of kerf width and surface roughness. Increase in kerf width (top and bottom) with increased water pressure and stand-off distance was reported, with insignificant effect of traverse speed. Wang and Guo [5] developed a semi-empirical predictive depth model based on the delamination in polymer matrix composites. Penetration depth was found to increase with decrease in jet traverse rate, pressure and abrasive flow rate (up to an optimum value). Shanmugam et al. [6] developed an empirical model to predict the kerf taper in AWJ machining of graphite/epoxy and glass epoxy composite laminates. High water pressure (280 MPa), low traverse speed (20 mm/s), and low standoff distance (2 mm) was recommended to achieve kerf taper angles below 2° and 6° for glass/epoxy and graphite/epoxy composite respectively. A comparative study of jetting technologies for composites machined at different angles 180°, 135°, 90°, and 45° concluded that minimum taper in AWJ machining of unidirectional aerospace composites can be achieved for straight cuts, and maximum for 45° angle due to inertial effects of nozzle traverse [7]. Conner et al. [8] studied the AWJ machining of thin aero-structural sheets of Inconel, titanium, aluminum and graphite/epoxy composite. A positive trend of average surface roughness was observed with traverse rate. Bottom kerf width was found significantly decreasing with traverse speed and slightly increasing with abrasive flow rate. The insignificance of fiber direction in machining composites was also reported. Mayuet et. al [9] studied the damages and delamination produced in 4 mm thick CFRP with weave type fiber reinforcement. They reported near-severe delamination with

increased abrasive flow rate (600 g/min) and intermediate traverse rate.
The aforementioned research studies provide an in-depth understanding of machining composite materials with pure waterjet and abrasive waterjet. However, one can expect dissimilarity in machining behavior for composites with randomly distributed short discontinuous fiber reinforcements as well as chopped discontinuous bundled fiber tapes. This assumption is broadly on the basis of the fact that conventional machining is influenced with fiber orientation, while abrasive and pure waterjet majorly influenced with the localized material heterogeneity. Limited studies have been conducted to fully understand the machinability of discontinuous composite materials. Briggs et al. [10] studied the AWJ edge finishing effects on the impact behavior of chopped GFRP composites. Due to the localized heterogeneity in the material, random cracks were generated under impact, extending in the direction of weakest areas – between and/or through the fiber bundled tapes. The AWJ specimens showed most localized damage with damage zone size 53% less than pure waterjet and 65% less than diamond saw cut. In discontinuous and chopped fiber composites, albeit, the material performance may show isotropic or quasi-isotropic behavior at macro scale, but meso-heterogeneity may play a pivotal role in the removal mechanism during the machining process. The heterogeneity arises from the disparate phases, and the possibility of "hot spots" due to air-entrapped regions and resin-rich pockets [11].

Knowing the advantages of high performance Discontinuous Fiber Composites, and the requirement of high speed machining for their potential infiltration in aerospace and automotive industry, there is no published work in open literature for machining of HexMC composite. The machinability is investigated in terms of material removal rate (MRR) and kerf taper. Material removal mechanism, and machining induced damages and defects are evaluated using optical and scanning electron microscopy. In addition, surface topography was studied to fully understand and characterize the jetting process for HexMC.

2. EXPERIMENTAL SETUP AND PROCEDURE

2.1 Materials

Rectangular plates of aerospace grade random fiber Carbon Epoxy HexMC® with thickness an approximate thickness of 10 mm was obtained. Due to improper control of the fabrication process, the bag side of the composite was uneven leading to thickness variation from 8 to 11 mm. HexMC consists of randomly oriented slit and chopped unidirectional prepreg tape (62% fiber weight content) chips of dimension: 50.8 mm x 8 mm. The mechanical properties are given in Table 1.

Table 1. Mechanical properties of HexMC.

Property	Value
Tensile Strength	300 MPa
Tensile Modulus	38 GPa
Flexural Strength	500 MPa
Flexural Modulus	30 GPa
Compression Strength	290 MPa
Compression Modulus	38 GPa
Interlaminar Shear Strength	250 MPa
Interlaminar Shear Modulus	15 GPa
Poisson's ratio	0.3

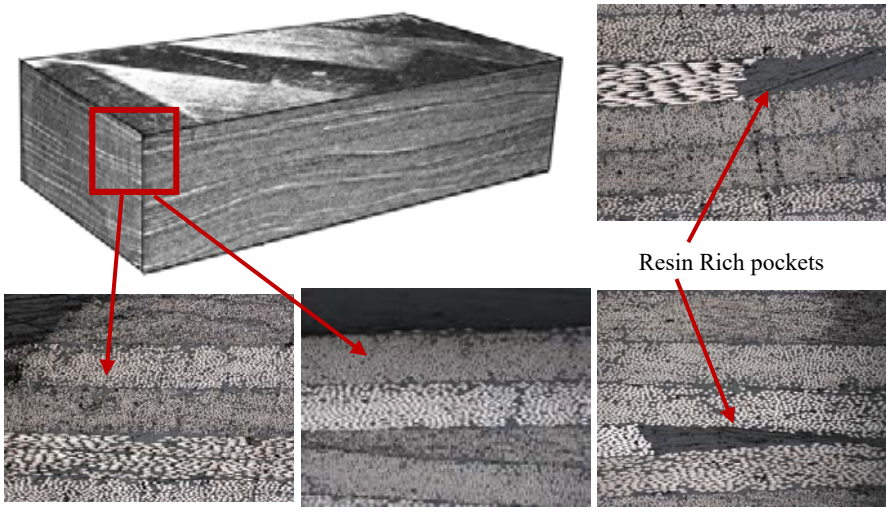

(a) (b)

Figure 1. Cross-sectional image of pristine HexMC, showing (a) Macro and microscopic view depicting random orientation of prepreg tapes; (b) Microscopic view of hot-spots (resin rich pockets)

2.2 Machining equipment

The abrasive waterjet experiments were performed using high pressure Flow International AWJ machine Model WJP 1313 equipped with 400 MPa intensifier. Table 2 provides the description of experimental conditions. The pump pressure, abrasive flow rate and jet traverse speed were selected according to industrial judgement and previous investigations on random fiber and unidirectional CFRP composites [2,12,13]. Orifice diameter to mixing tube diameter ratio used was 0.324, and mixing tube aspect ratio (length/diameter) was 100.

Table 2. AWJ Experimental conditions

Parameter	Description
Grit type	Garnet
Grit size (mesh#)	120
Impact angle	90°
Stand-off distance (mm)	1.0
Nozzle (mm)	Length 101.6 mm, Diameter: Ø 0.89 mm
Orifice (mm)	Diameter: Ø 0.33 mm, Ruby

The conventional trimming of HexMC was performed with HAAS® CNC milling machine with two flute carbide milling tool.

2.3 Experimental Design and Analysis

For abrasive waterjet, a fully crossed experimental design scheme was used in this study with 2 three-level factors and 1 four level factor, as outlined in Table 3, resulting in design matrix with 36 experimental runs. Optimal response surface design was used in 'Design-Expert v9.0.5' for Analysis of variance (ANOVA). The kerf width response was recorded at nine different jet penetration depths for each experimental condition, resulted in close to 324 measurements for ANOVA analysis.

Table 3. Experimental variable

Variable	Range
Jet Pressure (MPa)	250, 275, 350
Abrasive Flow rate (g/s)	5.3, 6, 6.8
Jet traverse speed (mm/s)	5, 10, 15, 19

The kerf surface was inspected using optical and scanning electron microscopy for the surface topology, morphology, defects and material removal mechanism. Further, to investigate and characterize the kerf topology, contact type surface profilometry was used with 2 µm probe and 5.6 mm evaluation length. Roughness parameters R_z (ten point average roughness) was primarily reported alongwith skewness and kurtosis because of their relevance to composite materials.

For conventional trimming operation, three levels of traverse feed rate – 5, 10, 15 mm/s and three levels of spindle speed –1000, 3000 and 6000 rpm was used to generate a total of 9 straight cuts.

1.1. Power density

The power density of pure waterjet stream jet is given by equation (1)

$$P_{wj} = C_d A_0 \sqrt{\frac{2}{\rho_w}} P^{1.5} \tag{1}$$

The power density of abrasive waterjet

$$P_{awj} = 0.5 \cdot \dot{m}_a \xi^2 \left(\frac{v_w}{1+R} \right)^2 \tag{2}$$

Now, the overall power efficacy of the conversion from waterjet to abrasive waterjet can be expressed by equation (4)

$$\text{Power efficacy } (\eta) = \frac{P_{awj}}{P_{wj}} \tag{3}$$

Substituting P_{wj} and P_{awj} from equations (1) and (2) yields equation (4)

$$\eta = \frac{R\xi^2}{(1+R)^2} \tag{4}$$

The abrasive waterjet power can now be expressed by substituting η from equation (4) and P_{wj} from equation (1) into equation (3)

$$P_{awj} = \frac{R\xi^2}{(1+R)^2} \cdot C_d A_0 \sqrt{\frac{2}{\rho_w}} P^{1.5} \tag{5}$$

The coefficient of drag C_d is assumed to vary linearly between 0.85 and 0.95 for pressure range 90–350 MPa.

3. RESULTS AND DISCUSSION

The machinability of HexMC was evaluated in terms of kerf width, surface roughness and material removal rate. Several contrasts between AWJ and conventional machining are apparent, as analyzed through a series of macro and micro inspection methods – surface profilometry, optical microscopy and Scanning Electron Microscope (SEM) inspection. These inspections also helped in characterizing the machining processes for HexMC composite.

3.1 Kerf width and geometry

The macro kerf features of AWJ machined randomly chopped composite are similar to AWJ machined quasi-isotropic carbon/epoxy composite. As shown in Figure 2(b), three cutting zones were identified: Initial damage, Smooth cutting and Rough cutting region. Figure 2 compares the kerf surfaces machined with different traverse speed and pressure at 5.3 g/s AFR. A low pressure and high traverse speed generated kerf surface with largest Rough cutting zone where abrasive jet, already low on energy, loses the cutting ability much sooner than the full penetration depth. This is reflected by the jet curving and resulting striated marks, with a growing declination angle towards the jet exit side. On the contrary, the low traverse and high pressure infused high power jet, resulting in smooth cutting region extended almost throughout the entire workpiece depth. The pressure increment from 200 MPa to 350 MPa improved the depth of smooth cutting zone irrespective of the traverse speed. However, a high pressure and low traverse speed sometimes resulted in interply macro-cracking and delamination at the matrix-prepreg interface. This effect is a possible coupled effect of high exposure and localized stagnation pressure during the cutting process, resulting in delamination of the weak bond near the jet exit side.

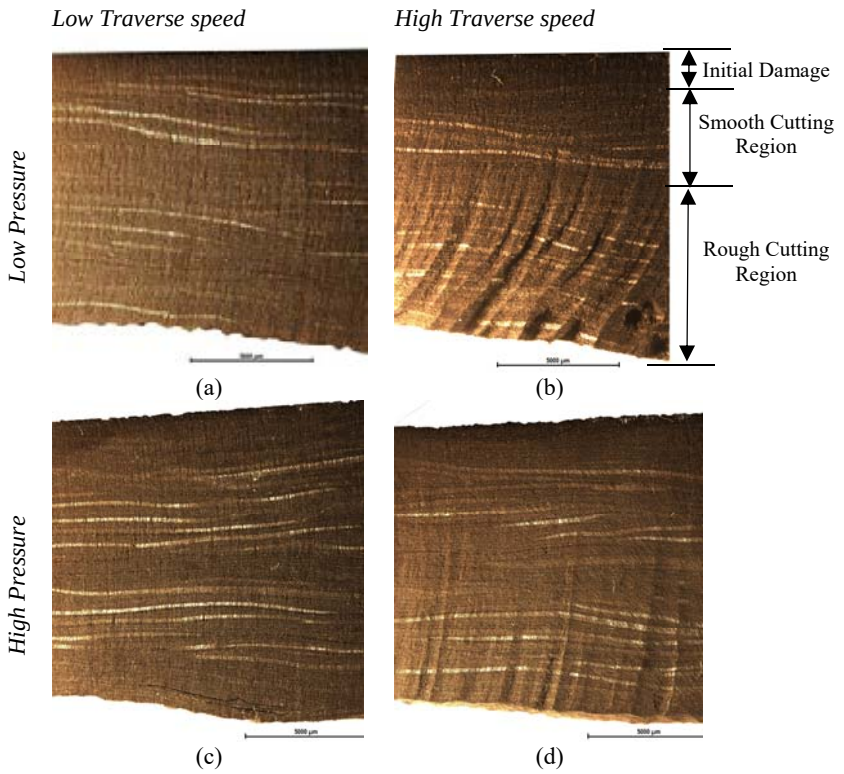

Figure 2. Optical images of AWJ machined kerf surface, machined with 5.3 g/s AFR and (a) Pressure=200 MPa, traverse speed=5 mm/s, (b) Pressure=200 MPa, traverse speed=19 mm/s, (c) Pressure=350 MPa, traverse speed=5 mm/s, and (d) Pressure=350 MPa, traverse speed=19 mm/s.

Typical kerf shape, as in Figure 3 observed was concave-type with Gaussian geometry at the jet entry side. As apparent, and reflected on kerf surface (in Figure 2b), low pressure and high speed resulted in loss of jet cutting ability with smaller kerf width. With the increased pressure, although the kerf overcut increased, but a near square cut was achieved. The initial damage region corresponds to the curved portion near the jet exit side. Visual inspection revealed that the spread of the initial curvature was predominantly affected by pressure level, and an increased pressure was required to reduce the initial damage. Figure 3(a) depicts the kerf shape at 5 mm/s and 200 MPa with initial damage zone extending up to 1.8 mm from the top surface. This zone was reduced to ~1 mm when pressure was increased to 350 MPa, as shown in Figure 3(c). Noticeably, the reduction in initial damage region with increased pressure was not prominent at high traverse speed. This can be attributed to the insufficient pressure buildup at low jet exposure time when the traverse feed rate is high.

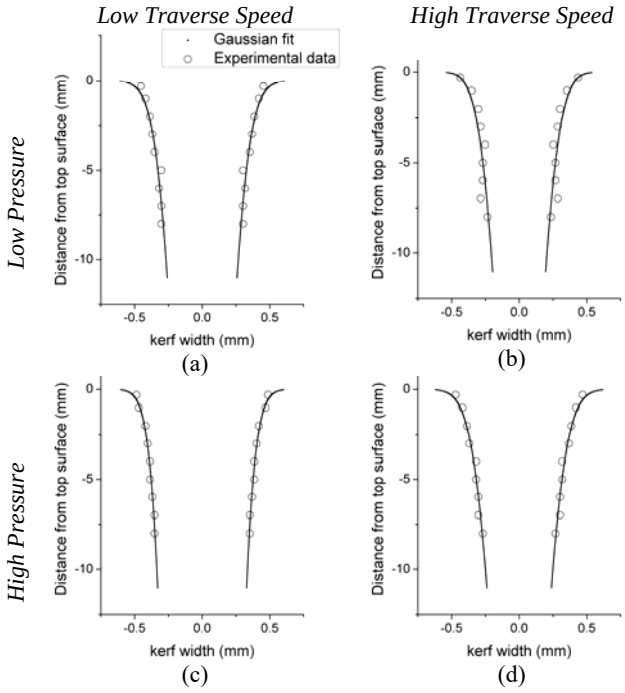

Figure 3. Kerf geometry of AWJ machined kerf surface, machined with 5.3 g/s AFR and (a) Pressure=200 MPa, traverse speed=5 mm/s, (b) Pressure=200 MPa, traverse speed=19 mm/s, (c) Pressure=350 MPa, traverse speed=5 mm/s, and (d) Pressure=350 MPa, traverse speed=19 mm/s.

The observed kerf width ranged between 0.484 –1.1 mm which is 0.48 to 1.24 nozzle diameters. ANOVA was used to develop regression model (Equation 6). As depicted in Figure 4(d), of all the parameters, penetration depth significantly affected the kerf width. Among the controllable process variables, traverse speed and pressure were the major contributive factors with 14.4% and 13.6% contribution.

$$\begin{aligned}\text{Kerf width (mm)} = {} & 0.854685 - 0.00297\ \dot{m}_a + 0.00065\ P - 0.08789\ \text{h} - 0.01513\ \text{u} \\ & + 0.001799\ \dot{m}_a h + 2\times10^{-5}\ Ph - 0.00091\ hu + 0.005465\ h^2 + 0.000422\ u^2\end{aligned} \quad (6)$$

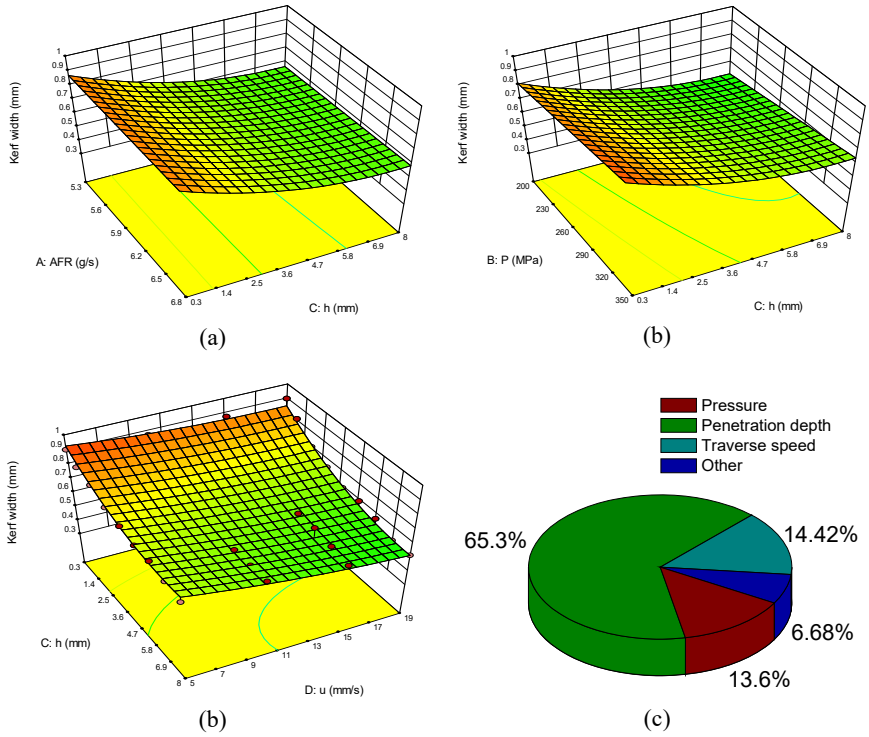

Figure 4. Kerf width as a function of (a) AFR and penetration depth, (b) pressure and penetration depth, (c) traverse speed and penetration depth, and (d) Contribution of factors in the model

Figure 4(a,b,c) depicts the interaction effect between penetration depth and other parameters. Kerf width showed a negative trend with penetration depth, traverse speed, and positive trend with pressure. About 30-35% reduction in kerf width was observed with increase in penetration depth from top surface to h=8mm. The effect of AFR was negligible for kerf width at low penetration depth, however, a small increase in kerf width was observed with AFR at high penetration depth.

The dependence of kerf width on the specific energy was plotted (Figure 5). Specific jet energy is defined as the ratio of inlet jet power to the volume rate at a given depth (Equation 7).

$$E_{sp,i} = \frac{P_{awj}}{u \cdot \int_{h=0}^{h_i} dA} \tag{7}$$

where P_{awj} is the abrasive waterjet power (from Equation 5), u is the traverse speed, A is the kerf cross sectional area from top to a given depth (h_i).

$$W / d_n = a_0 + a_1 e^{-E_{sp}/b_1}$$

$$a_0 = \text{-}8.247\text{e}8,\ a_1 = 2.324e7, b_1 = \text{-}0.08627$$

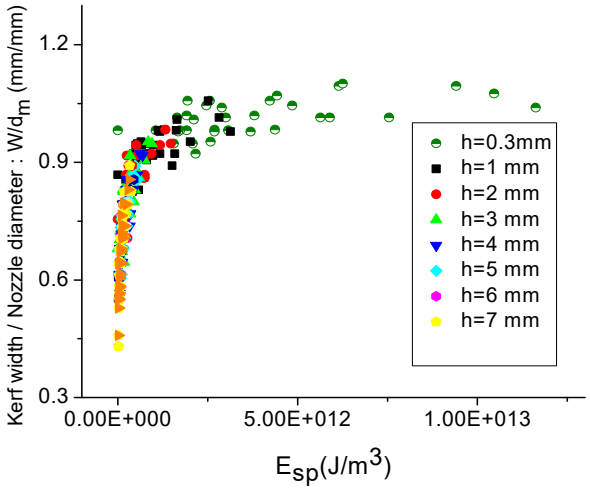

Figure 5. Ratio of kerf width and nozzle diameter as a function of specific energy.

The normalized kerf width depicted an exponential relationship with the specific cutting energy, as shown in Figure 5. At high specific energies (high jet power and at near-entry penetration depth), the kerf width is closest to the nozzle diameter, while it exponentially reduces at low specific energy levels. The energy of the jet is minimally expended when it is closer to the entry side. This is coupled with high power of the jet and hence, high cutting ability, resulting in kerf width nearly equivalent to the nozzle diameter. However, rapid energy loss during the jet-material interaction, especially at high penetration depth can be attributed to reduction of kerf width at low specific energies.

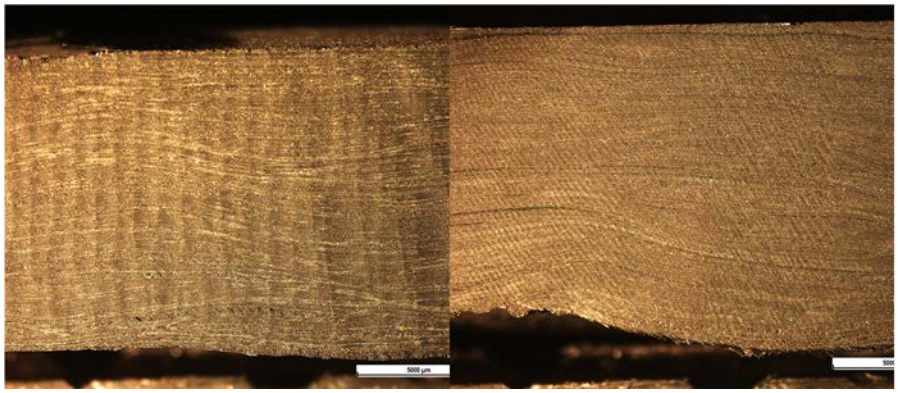

(a) (b)

Figure 6. Optical images of conventionally machined HexMC with (a) 15 mm/s traverse speed and 1000 rpm spindle speed, (b) 5 mm/s traverse speed and 6000 rpm spindle speed

Figure 6 (a) and (b) shows a typical kerf surface of conventionally trimmed HexMC machined with extreme conditions, corresponding to high and low surface roughness respectively. Figure 6(a) shows the kerf surface with high traverse feed (15 mm/s) and low spindle speed (1000 rpm) depicting regular tool feed marks, with macro damages spread throughout the kerf.

3.2 Surface Topology

The surface roughness was measured at every 1 mm interval, starting from the jet entry side for AWJ cut. However, due to consistency in the roughness values for conventionally machined specimens, the interval was 2 mm starting from the top. Within the range of experimental conditions used in this study, the surface roughness R_z for AWJ machined HexMC ranged between 19.3–83.8 µm, while conventionally machined roughness was over 60% lower and ranged between 6.7–34.8 µm.
The roughness parameter R_z demonstrated a strong relationship with the specific jet energy. This reveals that the surface topology and the cutting ability of the jet during the jet-material interaction process are strongly correlated.

$$R_z = a_0 + \sum_{i=1}^{3} a_i e^{-E_{sp}/b_i}$$

$$a_1 = 23.4,\ a_2 = 4.3\text{e}22,\ a_3 = 10.4$$

$$b_1 = 2.18\text{e}10,\ b_2 = 3.4\text{e}8,\ b_3 = 3.11e11$$

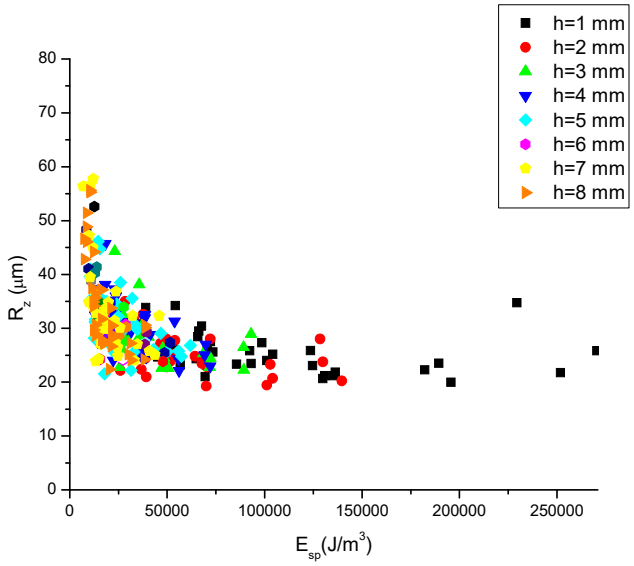

Figure 7. Roughness R_z (µm) as a function of specific energy

Another two important parameters –Skewness and kurtosis are analyzed. A negatively skewed profile has deep valleys in smoother plateaus, while a positively skewed profile has spiky protuberances in flatter surfaces. Processes such as milling, abrasive

machining, grinding, etc. are negatively skewed and reflect the effect of unit events generating the profile (random abrasive action causing micro-removal). Processes such as turning, EDM and sometimes milling generate positively skewed profile. Kurtosis is the measure of peakedness of the asperities and grooves. A topography generated by random action is Gaussian, and hence zero skewed with kurtosis=3. As seen in Figure 8, the topography generated by both conventional and abrasive machining are dominantly between zero and negative skewness.

The AWJ machined profiles, as observed from Figure 8(a) are cluttered near zero skewness with average kurtosis close to 3. This is a depiction of the near-Gaussian profile generated by micro-cutting and micro-removal by random abrasives. Interestingly, positive skewness with high kurtosis was predominantly observed at high jet penetration depths (h>4 mm). This reveals that the reduced cutting ability of the jet as it reaches the exit side causes delamination, fiber pull-outs, and other out-of-plane micro-defects and damages. The conventionally machined profiles exhibited negative skewness and were highly leptokurtic (Kurtosis>3). This is an indicator of severe micro-damages and fiber pull-outs in conventional machining.

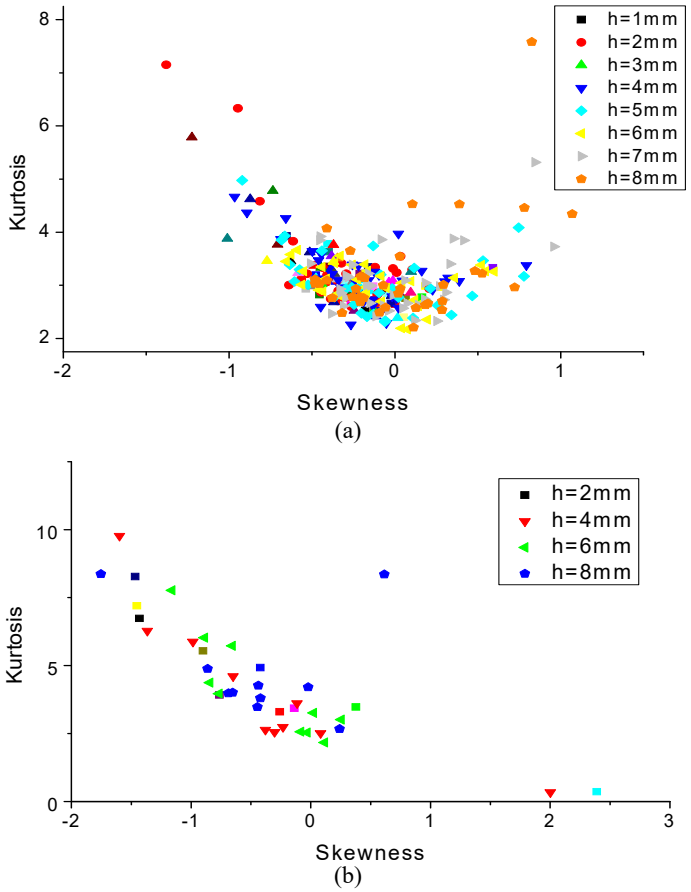

Figure 8. Skewness vs Kurtosis for (a) AWJ machined, (b) Conventionally machined HexMC.

3.3 Material Removal Rate

The material removal rate for Abrasive Waterjet was found within 4.72 and 51.8 mm^3/s, with traverse speed as the dominant contributing factor. ANOVA was used to develop predictive, regression model (Equation 8). The contribution of traverse speed was 83% of all the parameters used. Figure 9(a) shows the interaction effect of traverse speed and AFR on MRR. MRR shows a positive trend with the traverse speed at all abrasive flow rates. At low AFR (5.3 g/s), 364% increase in MRR is observed with the increment in traverse speed from 5 mm/s to 19 mm/s, which becomes 759% at high AFR (6.8 g/s). The trend also suggests that at low traverse rate, high AFR is not beneficial and can lead to ½ the MRR as with low AFR. This is because the possible overcut due to high jet exposure time is overcompensated by the increased jet cutting ability due to high AFR. Figure 9(b) shows the interaction effect of traverse speed and pressure on MRR. The increment of MRR is 400% and 700% with traverse speed at high and low pressure levels respectively.

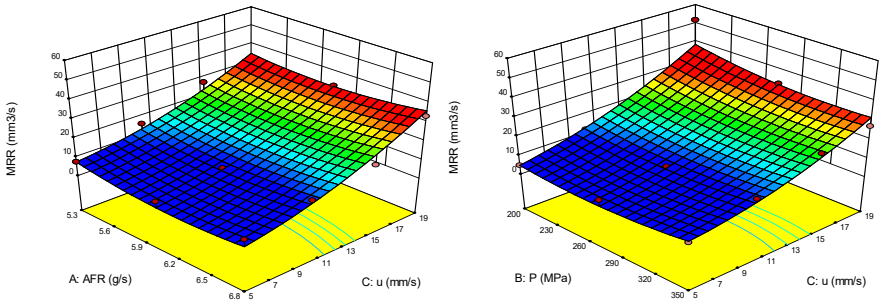

(a) (b)

Figure 9. Material Removal Rate (MRR) as a function of (a) AFR and traverse speed, and (b) Pressure and traverse speed.

$$MRR\left(mm^3/s\right) = 260.014 - 72.3042\,\dot{m}_a - 0.25565\,P - 0.15436\,u + 0.000681\,\dot{m}_a P + 0.212638\,\dot{m}_a u - 0.00412\,Pu + 5.68889\,\dot{m}_a^2 + 0.000513\,P^2 + 0.088362\,u^2 \quad (8)$$

Figure 10 shows the relation between Material removal rate and Roughness R_z. R_z is plotted as an average of eight values measured on the kerf surface at different jet penetration depths. Since the average of these values may not be a good indicator of severity, standard deviation is plotted as error bars. It can be observed that not only the surface becomes rougher when machined with conditions leading to higher material removal rate, but the spread of the roughness values from jet entry to jet exit also increases. The lowest MRR (23.24 mm3/s) corresponds to smoother surface with R_z =4.74 µm, while 90.1% increment in roughness was observed with 993% increase in MRR. Besides, the standard deviation of roughness varies from 2.5 to 18.8 from low to high MRR. It can be observed from figure 10 that standard deviation of roughness shoots up when MRR is greater than 20 mm/s. The maximum deviation is 7.1 for R_z=34.5 µm and MRR< 20mm^3/s.

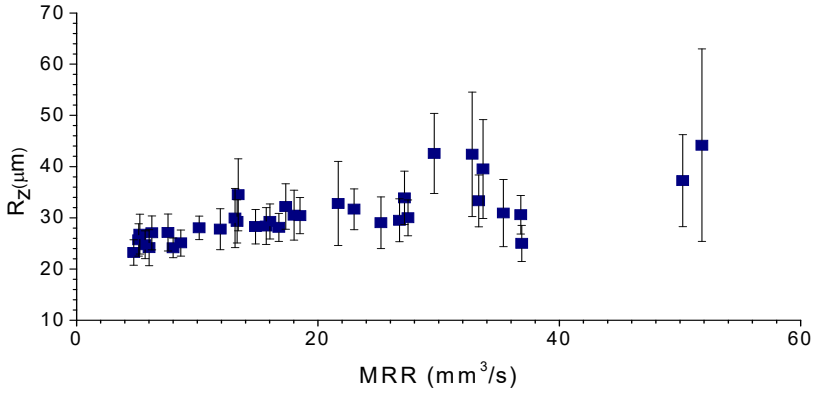

Figure 10. Roughness R_z as a function of Material Removal Rate (MRR)

The MRR for conventional machining varied between 700-2100 mm/s. However, a direct comparison between the MRR for AWJ and conventional machining is an inappropriate approach due to difference in tool diameter and cutting quality achieved. Since the AWJ nozzle diameter is 0.88 mm as opposed to 12.7 mm diameter cutting tool, it can be employed to machine the 12.7 mm wide cut geometry as a slot. This would lead to MRR for AWJ as 15 times higher than conventional. However, a better comparative parameter would be kerf surface quality as a function of traverse speed.

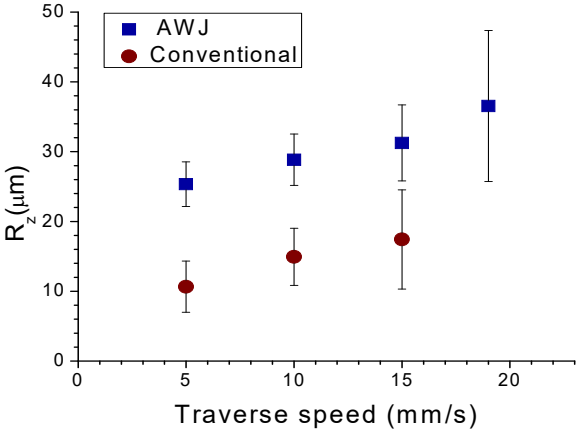

Figure 11. Comparison of R_z dependence on traverse speed for AWJ and conventional machining

Figure 11 shows the average roughness R_z parameter as a function of tool traverse speed/ traverse feed rate. It can be observed that for any given speed, roughness R_z was higher for AWJ when compared to conventional machining. This is attributed to the removal mechanisms involved in the two machining processes. The high temperature involved in the conventional machining process leads to smearing of the matrix material and thermal degradation, resulting in covering the machining induced damage, and hence low roughness [14]. However, the severity of sub-surface damage may be high enough to affect the microstructural integrity [15,16]. The reasoning is congruent with the photo-

micrographic evidence discussed in Section 3.4 where a few pockets of fiber bundles and other micro-defects are observed in the dominant smeared matrix. The average roughness R_z for Abrasive waterjet is 138% higher than conventional at 5 mm/s traverse speed. The difference is 80% when traverse speed goes up to 15 mm/s. This is because of the possible reduction in matrix smearing at high traverse rate due to less exposure time of the cutting edge to cause thermal distortion.

3.4 Microstructural characteristics

The surface characteristics of AWJ and conventionally machined specimens are inspected through scanning electron microscopy. The arrow on the top left of each micro-photograph depicts the cutting tool feed or jet traverse direction for conventional and AWJ machining respectively.

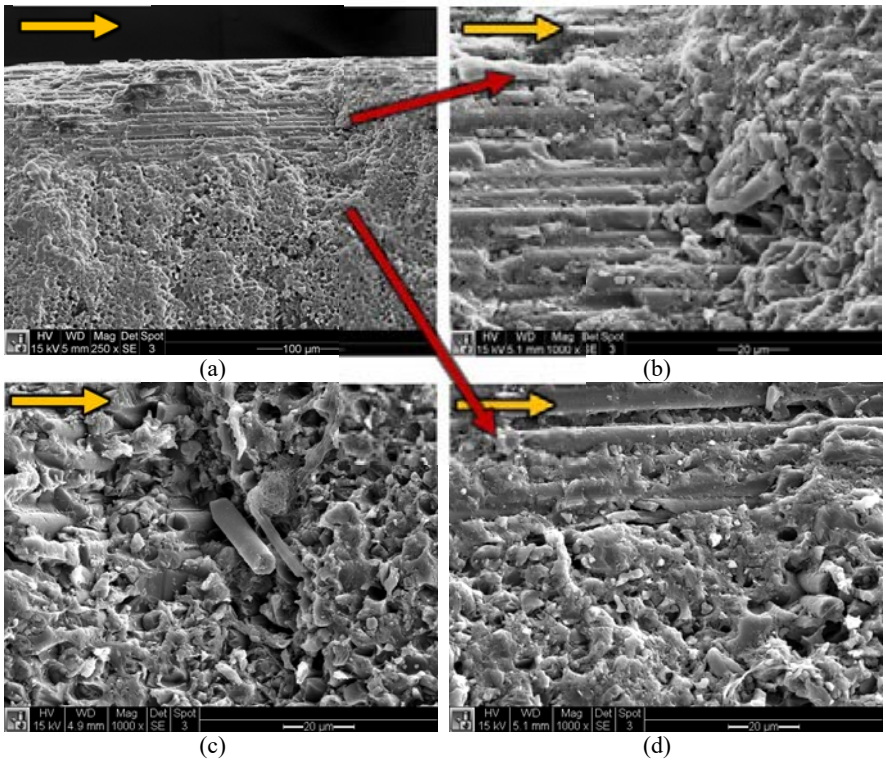

Figure 12. SEM photo-micrographs of the top and near top kerf surface of AWJ machined specimen, machined with 5.3 g/s AFR, 200 MPa pressure and 19 mm/s traverse speed, depicting (a) Damage at jet entry, (b) Wear tracks, (c) Fiber breaking (d) Near-orthogonal fiber breaking.

The top surface of the AWJ machined specimens showed surface with near-parallel fibers completely exposed at certain regions. The fibers oriented near-parallel to the jet traverse direction showed abrasive wear tracks as a typical characteristic. As evident from Figure 12(a), these wear tracks were limited to about 120-150μ depths, 13-20 fiber

diameters or 1-1.3 times the abrasive size. The reason for these wear tracks is believed to be the action of stray abrasives slinging at the exterior of the jet, causing fiber roll-outs at the end of these tracks (Figure 12(d)). However, the degree of fiber roll-out is very low when compared to exit side. The initial damage is attributable to the high degree of micromachining by sharp cutting edges of the abrasives. Figure 12(b) shows the sharp abrasive marks with semi-split fibers, and very small sized debris captured in the wear track. The fibers oriented near-orthogonal to the jet traverse direction witnessed bending and shearing as the primary erosion mode, as apparent from Figure 12(d). Fiber pull outs (withdrawal of fibers from matrix pockets) were also seen, but coupled with bending and breaking. Typical pulled out fibers were about 40-50µ long (5-7 times fiber diameter), as seen in Figure 12(c).

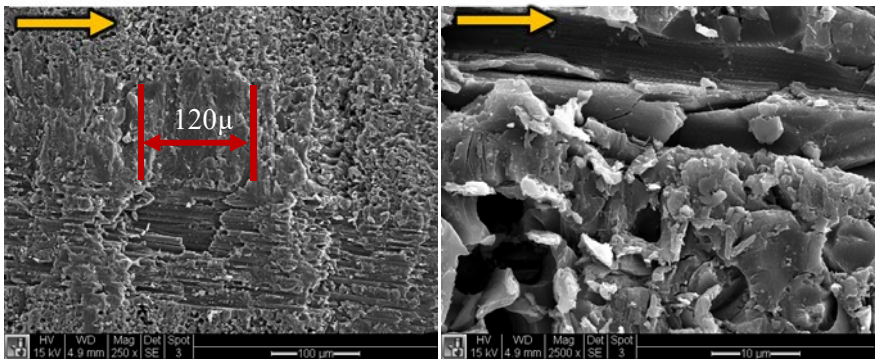

(a) (b)

Figure 13. SEM photo-micrographs of the middle kerf surface of AWJ machined specimen, machined with 5.3 g/s AFR, 200 MPa pressure and 19 mm/s traverse speed, depicting (a) wear track (b) dependence of removal mechanism on fiber orientation.

Halfway through the jet penetration depth, resin rich areas were found to be plastically deformed. As depicted in Figure 13(a), severe plastic deformation of the matrix was followed by fracturing rolling-out of the near parallel fibers. The size of the deformed zone was ~120 µm, suggesting the action and footprint of single abrasive. Figure 13(b) depicts the photomicrograph within an area of about 0.5 times the abrasive size. Within this area three different fiber orientations are covered, with several different removal mechanisms. The near parallel fibers are fractured with an inclined fracture plane, and sometimes rolled out. The near-orthogonal fibers are under the action of combined loading –bending and shearing, coupled with micromachining. Fiber pull-outs were also observed for this near-orthogonal orientation, but the frequency and degree of pull-outs is lesser when compared to jet entry and exit side. Clearly, there is a strong contingency of fiber orientation on the removal mechanisms even in small areas where probability of single abrasive action is high. Matrix surrounding the fibers was mostly intact.

Towards the jet exit side, the striated zone becomes prominent along with features of jet deflection in backwards direction. Figure 14(a) and (b) depicts shows the striated region which spreads out towards the exit side. The gouged region is about 40–100µm deep, 12-13 times fiber diameter. Several small grooves can be seen in the striated gouge, which possibly depict the action of water. Delamination was primarily found near the jet exit side, 2-15 fiber diameters from the bottom, as seen in Figure 14(c). This can be attributed to the combined effect of low energy jet causing the jet spreading, weak resin material and lack of support by the underneath layers towards the bottom.

Interestingly, the delamination sites were not prominent in the prepeg chip-epoxy interface, and that the matrix material was intact, with fibers bundled together. This shows the strong bonding of prepreg layers. The jet not only loses the cutting ability, but the jet structure itself changes, catapulting the low energy abrasive particle into the material. Figure 14(d) depicts the embedded abrasive particle which leads to crack generation and propagation. The reduced size (1/4 – 3/4th of pristine abrasive size) of the abrasive with multiple sites of brittle fractures depict the loss of sharp edges in degradation of abrasive in focusing tube and in the cutting interaction process.

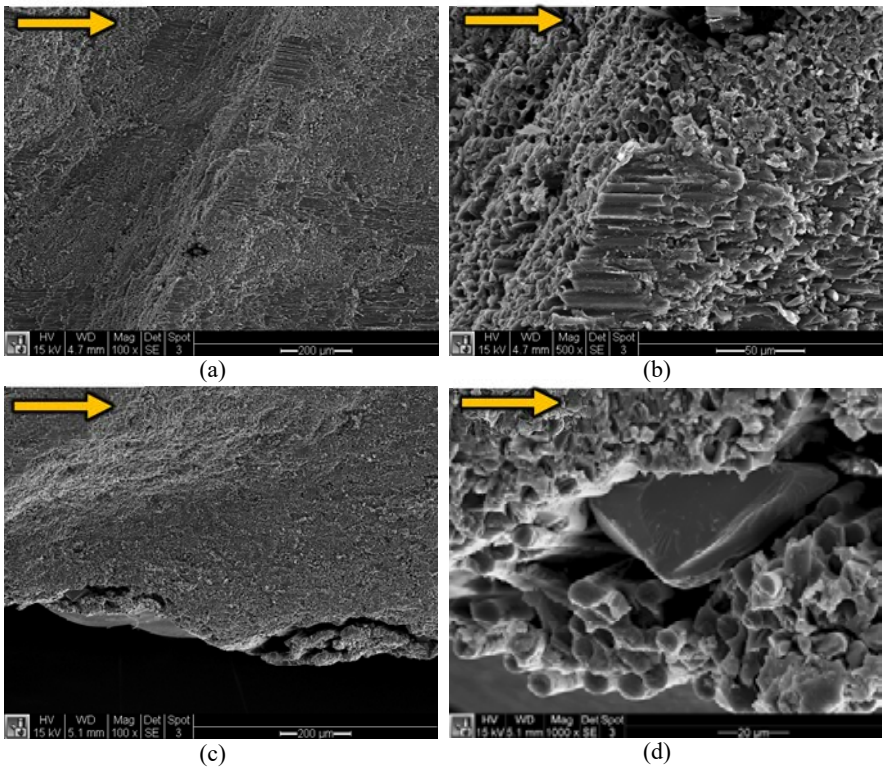

Figure 14. **SEM photo-micrographs of the top and near top kerf surface of AWJ machined specimen, machined with 5.3 g/s AFR, 200 MPa pressure and 19 mm/s traverse speed, depicting (a) striated groves, (b) magnified image of striated zone, (c) Exit delamination (d) Abrasive embedment near jet exit.**

Whilst the jet energy is low at the bottom, the inclined fibers continued to be removed by brittle fracturing and micro-cutting, with matrix intact. As compared to low pressure condition (Figure 12(a)), the initial damage surface (wear grooves) becomes deeper and more frequent when compared with surface machined with high pressure condition (Figure 15(b)). Upon comparing surfaces machined with low traverse speed (5 mm/s) and high traverse speed (19 mm/s), it is apparent from Figure 15(a) and (b) respectively that the wear tracks becomes deeper, shorter and more frequent with the increase in traverse rate.

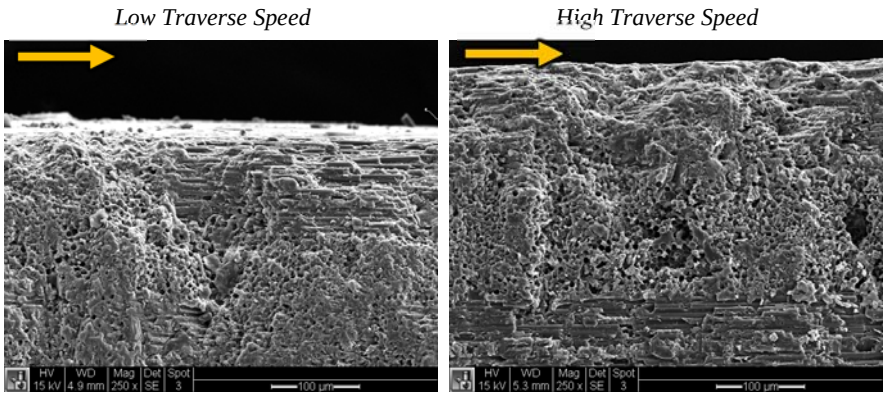

(a) (b)

Figure 15. SEM photo-micrographs of the top surface of AWJ specimen, machined with 5.3 g/s AFR, 350 MPa pressure and traverse speed (a) 5 mm/s, (b) 19 mm/s.

Figure 16(a) and (b) illustrate the near-exit delamination of AWJ specimens machined with 5mm/s and 19 mm/s traverse speed respectively. It can be seen that the material delaminates at 10–15 fiber heights from the bottom surface for 5 mm/s. However, at high traverse speed (19 mm/s), the delamination was severe, more frequent and occurred about 20–25 fiber heights from the bottom surface. Besides, at high traverse rate, hackle pull out of fibers was observed near the jet exit side. The near-orthogonal fibers were pulled out in localized bunches resulting in low matrix density.

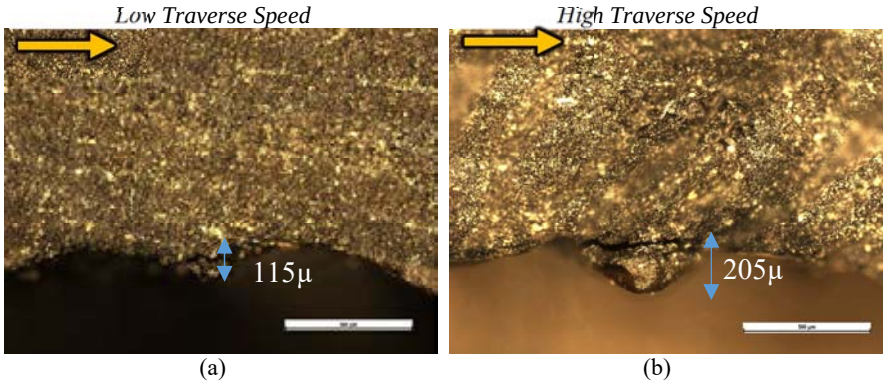

(a) (b)

Figure 16. Optical micrographs of the bottom surface of AWJ machined specimen, machined with 5.3 g/s AFR, 200 MPa pressure and traverse speed (a) 5 mm/s, (b) 19 mm/s.

Sometimes, at high pressures and low traverse speeds, unusually high delamination was observed. Figure 17(a) shows one such case where the delamination occurred along prepreg-matrix boundary, as well as abrasive intrusion within the prepreg chip. This can be attributed to the coupled effect of low prepreg chip-matrix interfacial bond strength, high pressure and slow speed, resulting in high exposure time. This slow material removal process adds up to the already high localized pressure. The resulting jet impacts the material in out-of-plane direction, and leading to material failure by water and abrasive intrusion into the kerf rather than micro-machining.

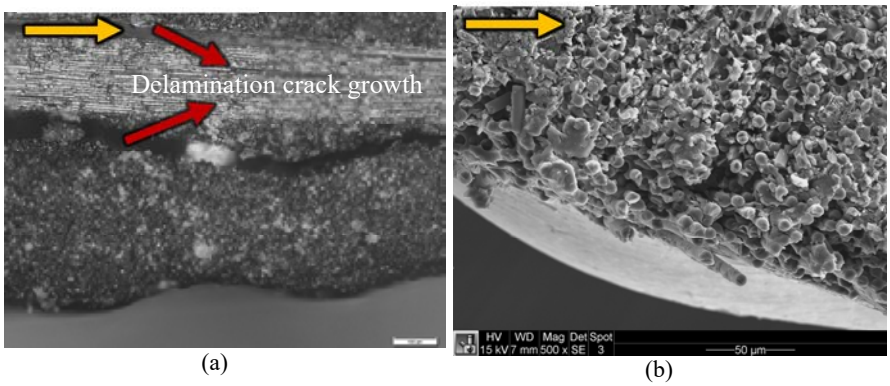

(a) (b)

Figure 17. (a) Optical micrograph of AWJ machined specimen with 5.3 g/s AFR, 350 MPa pressure and 5 mm/s traverse speed depicting delamination and crack growth, (b) SEM micrograph of jet exit side of AWJ machined specimen, machined with 6.8 g/s AFR, 350 MPa pressure and 19 mm/s traverse speed.

Specimens machined with high abrasive load depicted a smoother topology. Figure 17(b) illustrates one such case where degree of delamination, fibers pull out density was low. Matrix around the fibers was intact, suggesting micro-cutting as dominant mode of material removal even at high penetration depth.

Conventionally machined HexMC was also inspected through SEM micro-photographs. The conditions resulting in high roughness (high feed, low speed) and low roughness (low feed, high speed) were selected for the SEM inspection, as shown in Figure 10(a),(c),(e) and Figure 10(b),(d),(f) respectively. High degree of type I and type II [17] delamination was observed at the top surface where the uncut fibers from the surface plies protrude. The length, width and occurrence of this top surface delamination is dependent on the relative angle between the cutting edge of the tool and fiber direction. At high traverse feed rate and low spindle speed, the top ply delamination was maximum with bunch pull-outs extended up to 300 µm from the top surface. The top surface damage height reduced to about 1/3rd when machined with low traverse and high spindle speed. Machined surface with high traverse and low spindle speed resulted in fiber pull-outs, especially for near 135° fiber–tool edge relative angle. However, the other fiber orientations were smeared with the matrix. The degree of matrix smearing and thermal degradation was high in specimens machined with low traverse and high speed. Overall, the matrix smearing resulted in smoother surface for conventional milling when compared to AWJ, but far more severe damage locations were identified near top and bottom edge. It is believed that the sub-surface damage is likely to be higher beneath the smeared matrix on the kerf surface. This macro and micro damage is only visible at top, bottom and for near 135° fiber orientations.

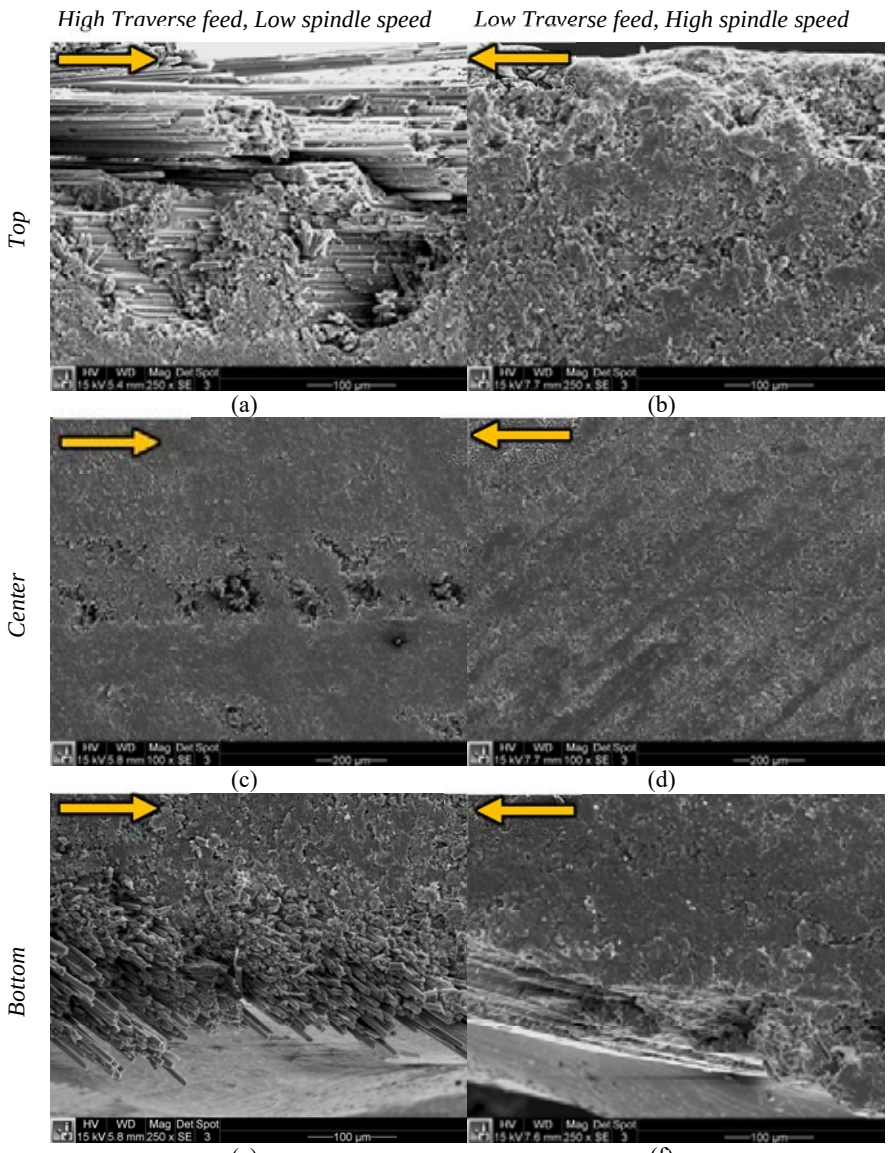

Figure 10. SEM photo-micrographs of conventionally trimmed HexMC, machined with 15 mm/s, 1000 rpm depicting (a) Top, (c) Center, (e) Bottom surface, and machined with 5mm/s, 6000 rpm depicting (b) Top, (d) Center, and (f) Bottom surface.

4. SUMMARY AND CONCLUSION

The machinability of high performance, randomly chopped, CFRP prepreg/epoxy Discontinuous fiber composite (DFC) was evaluated through abrasive waterjet and conventional milling processes. The machinability was evaluated in terms of kerf width and geometry, surface topology, material removal rate and micro-structural characteristics generated by different machining parameters. For Abrasive Waterjet water pump pressure was varied between 250 and 350 MPa, traverse speed between 5 and 19 mm/s and abrasive flow rate between 5.3 and 6.8 g/s. The milling operation was performed with 12.7 mm diameter carbide tool with traverse feed rate between 5 and 15 mm/s, and spindle speed between 1000 and 6000 rpm. The parametric dependence of the machining responses were studied both empirically and as a function of specific energy. ANOVA was used to generate predictive regression models for MRR and kerf width. Based on the investigation, following conclusions were made:

1. AWJ resulted in variable kerf width as opposed to conventional trimming. Cutting tool to kerf width ratio was 0.48–1.24 for AWJ and nearly 1.0 for conventional machining. The kerf width showed an exponentially growing relation with specific jet energy. Small kerf width was observed at low specific energy (low pressure, high traverse speed, low abrasive flow rate and high penetration depth).

2. AWJ resulted in rougher surfaces with R_z between 19.3–83.8 μm, as opposed to conventional machining which resulted in over 60% lower roughness, ranging between 6.7–34.8 μm. When compared with same traverse speed, roughness variation between AWJ and conventional was 80–140%. Both AWJ and conventionally generated surface profiles were leptokurtic with AWJ surface topology was predominantly zero to negatively skewed, while conventionally generated surface was strongly skewed negatively.

3. AWJ shows a conspicuous surface topology, as opposed to conventional machining where the machining induced damage is concealed beneath the smeared matrix, but occasionally visible at the top and bottom side, and near 135° ply orientations. Wherever visible, the damage appeared to be much more severe than AWJ.

4. AWJ involved several different removal mechanisms. Fibers were removed by shearing and micro-machining, brittle fracturing and micro-cutting, and bulk erosion, depending on the fiber orientation. Matrix was mostly removed by shearing and sometimes bulk erosion. Machining characteristics for conventional were highly dependent on fiber orientation.

5. For AWJ, delamination was predominantly found near the jet exit side. Unlike Unidirectional laminate, the delaminated crack length was restricted because of the discontinuous prepreg chips. Most delamination sites were within 10-15 fiber heights from bottom at low traverse speed, but 25-30 fiber heights at high traverse speed. Severe delamination was observed for conventionally machined HexMC with uncut fibers protrusion near the top side.

REFERENCES

[1] Boeing 787 features composite window frames. Reinf Plast 2007;51:4. doi:http://dx.doi.org/10.1016/S0034-3617(07)70095-4.

[2] Ramulu M, Arola D. Water jet and abrasive water jet cutting of unidirectional graphite/epoxy composite. Composites 1993;24:299–308. doi:10.1016/0010-4361(93)90040-F.

[3] Hashish M. Waterjet Machining of Advanced Composites. Mater Manuf Process 1995;10:1129–52. doi:10.1080/10426919508935098.

[4] Wang J. A machinability study of polymer matrix composites using abrasive waterjet cutting technology. J Mater Process Technol 1999;94:30–5. doi:http://dx.doi.org/10.1016/S0924-0136(98)00443-9.

[5] Wang J, Guo DM. A predictive depth of penetration model for abrasive waterjet cutting of polymer matrix composites. J Mater Process Technol 2002;121:390–4. doi:10.1016/S0924-0136(01)01246-8.

[6] Shanmugam DK, Masood SH. An investigation on kerf characteristics in abrasive waterjet cutting of layered composites. J Mater Process Technol 2009;209:3887–93. doi:10.1016/j.jmatprotec.2008.09.001.

[7] Shanmugam DK, Chen FL, Siores E, Brandt M. Comparative study of jetting machining technologies over laser machining technology for cutting composite materials. Compos Struct 2002;57:289–96. doi:10.1016/S0263-8223(02)00096-X.

[8] Conner I, Hashish M, Ramulu M. Abrasive waterjet machining of aerospace structural sheet and thin plate materials. Proc. 2003 WJTA Am. Waterjet Conf. Houston, Texas, 2003, p. 17–9.

[9] Mayuet PF, Girot F, Lamíkiz A, Fernández-Vidal SR, Salguero J, Marcos M. SOM/SEM based Characterization of Internal Delaminations of CFRP Samples Machined by AWJM. Procedia Eng 2015;132:693–700. doi:10.1016/j.proeng.2015.12.549.

[10] Briggs TM, Ramulu M. Edge Finishing Effects on the Impact Behavior of Chopped GFRP Composites. Exp Mech 2010;50:321–31. doi:10.1007/s11340-009-9235-8.

[11] Feraboli P, Cleveland T, Ciccu M, Stickler P, DeOto L. Defect and damage analysis of advanced discontinuous carbon/epoxy composite materials. Compos Part A Appl Sci Manuf 2010;41:888–901. doi:10.1016/j.compositesa.2010.03.002.

[12] Ramulu M, Arola D. The influence of abrasive waterjet cutting conditions on the surface quality of graphite/epoxy laminates. Int J Mach Tools Manuf 1994;34:295–313. doi:10.1016/0890-6955(94)90001-9.

[13] Shanmugam DK, Masood SH. An investigation on kerf characteristics in abrasive waterjet cutting of layered composites. J Mater Process Technol 2009;209:3887–93. doi:10.1016/j.jmatprotec.2008.09.001.

[14] Ramulu M, Wern CW, Garbini JL. Effect of fibre direction on surface roughness measurements of machined graphite/epoxy composite. Compos Manuf 1993;4:39–51. doi:http://dx.doi.org/10.1016/0956-7143(93)90015-Z.

[15] Arola D, Ramula M. Machining-induced surface texture effects on the flexural properties of a graphite/epoxy laminate. Composites 1994;25:822–34. doi:http://dx.doi.org/10.1016/0010-4361(94)90143-0.

[16] Ramulu M. Machining and surface integrity of fibre-reinforced plastic composites. Sadhana 1997;22:449–72. doi:10.1007/BF02744483.

[17] Colligan K, Ramulu M. The effect of edge trimming on composite surface plies. Manuf Rev 1992;5:274–83.